



Efficient machine learning approach for accurate free-energy profiles and kinetic rates

Timothée Devergne 

*Institut de Minéralogie, de Physique des Matériaux et de Cosmochimie, UMR 7590 CNRS, Sorbonne Université,
Muséum National d'Histoire Naturelle - Paris 75005, France;*
Atomistic Simulations, Italian Institute of Technology, 16142 Genoa, Italy;
and Computational Statistics and Machine Learning, Italian Institute of Technology, 16142 Genoa, Italy

Leon Huet , Fabio Pietrucci, and A. Marco Saitta 

*Institut de Minéralogie, de Physique des Matériaux et de Cosmochimie, UMR 7590 CNRS, Sorbonne Université,
Muséum National d'Histoire Naturelle - Paris 75005, France*



(Received 6 November 2023; accepted 1 August 2024; published 3 September 2024)

The computational exploration of reactive processes is challenging due to the requirement of thorough sampling across the free energy landscape using accurate *ab initio* methods. To address these constraints, machine learning potentials are employed, yet their training for this kind of problem is still a laborious and tedious task. In this study, we present an efficient approach to train these potentials by cleverly using a single batch of unbiased trajectories that avoid the pitfalls of trajectories artificially biased along a suboptimal collective variable. This strategy, when integrated with current enhanced sampling techniques, allows to obtain free energy profiles and kinetic rates of *ab initio* quality, yet dramatically reducing the computational cost.

DOI: [10.1103/PhysRevE.110.L033301](https://doi.org/10.1103/PhysRevE.110.L033301)

Introduction. Atomistic computational studies of chemical reactions in solution are essential for gaining a comprehensive understanding of their complexity and underlying microscopic mechanisms. The primary aim is to accurately describe the reactive process, enabling the recovery of crucial kinetic and thermodynamic information [1,2]. This information can be compared with experimental data to enhance our understanding of laboratory-observed reactions and provide valuable guidance to experimentalists. To validate identified mechanisms, computational results must be compared with experimentally measured equilibrium constants and kinetic rates. However, computing these quantities poses significant challenges.

To address the challenge of time limitations in simulations compared to experimental reaction times, several enhanced sampling techniques are typically employed [3], such as metadynamics [4] and umbrella sampling (US) [5]. In our previous studies [6–8], metadynamics is used as an exploratory tool, allowing for the exploration of the first transition trajectory between two metastable states. We subsequently employ US to sample the free energy landscape by projecting the reaction mechanism onto a collective variable (CV), divided into narrow bins. From these calculations, we obtain the free energy profile along the sampled path, thus providing crucial information about the free energy difference between reactants and products and the activation barrier. The free energy difference (ΔF^0) directly correlates to the equilibrium constant (K) through an exponential relation at inverse temperature β : $K = \exp(-\beta\Delta F^0)$. However, accurately obtaining the kinetic rate poses challenges and often relies on the reactive flux formalism [9], demanding significant statistical sampling, or on less-accurate transition state (TS) theory.

To perform the CV projection in a kinetically meaningful way, a comprehensive understanding of the targeted mechanism is essential. Transition path sampling (TPS) and its variants [10] serve as valuable techniques for gathering information about the mechanism. TPS samples the transition path ensemble by performing numerous relaxation trajectories starting from the top of the free energy barrier, faithfully reproducing (at convergence) reactive trajectories that would be observed in unbiased, unfeasibly long simulations. TPS has been recently used to extract free-energy landscapes and rates from optimal Langevin models [11], as well as to identify optimal CVs [12–15]. In this work, we adopt the TPS variant called “shooting from the top” [16]. Due to the considerable number of trajectories needed to explore the transition path ensemble and devise a CV, the use of *ab initio* molecular dynamics (AIMD) calculations with this technique remains limited, often favoring heuristic reaction-dependent CVs to reduce computational costs. Moreover, obtaining high-quality kinetics necessitates a vast number of transition trajectories. Thus, achieving a balance between a good TPS-based CV, accurate statistical sampling, and reliable kinetics poses a challenge [13].

To address the computational cost problem associated with reactive rare events, researchers have developed machine learning interatomic potentials (MLIPs) [17–21]. MLIPs learn the potential energy surface (PES) from *ab initio* atomic configurations, energies, and forces, enabling AIMD-quality molecular dynamics at a reduced computational cost. MLIPs have shown great promise in expanding the reachable time and length-scales of equilibrium systems [22] and reducing the computational cost of simple systems [23]. However, building MLIPs for reactive rare events is more challenging, as the

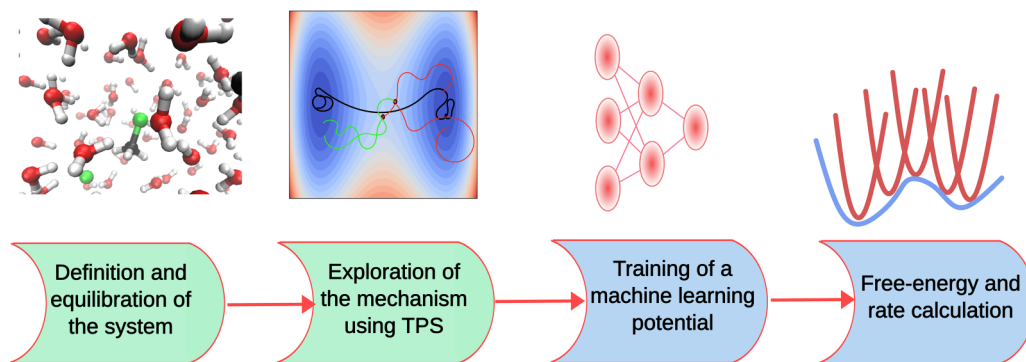


FIG. 1. Computational protocol proposed in this study: first the system is equilibrated, then *ab initio* TPS simulations are run to train a machine learning potential that is in the end used to compute free-energy landscapes (umbrella sampling) and kinetic rates (reactive flux).

training set must sample the entire reactive space, including configurations where the system is out of equilibrium, i.e., very unlikely and unstable configurations that are not accessible using unbiased molecular dynamics alone. To overcome this problem, researchers have devised methods to train MLIPs from biased trajectories which requires the definition of a CV and hence, the prior knowledge of the transition mechanism [8,24–26], but the use of the MLIPs is often restricted to one usage in the sampling protocol. On the other hand, TPS simulations produce unbiased trajectories starting from the top of the barrier and ending in the equilibrium basins, i.e., including valuable information about the whole reaction path. Even though a first reactive trajectory is needed to initialize TPS, the algorithm subsequently finds automatically, in an iterative way, the most probable transition states. TPS thus avoids the negative effects of using a suboptimal CV in biased methods, that potentially lead to reactive trajectories sampling unlikely configurations, different from unbiased ones. This is why MLIPs in combination with unbiased TPS data are a promising solution to the computational cost issue as well as to the accuracy issue, facilitating predictions of kinetics and thermodynamics at the *ab initio* level in reactive systems.

Building on previous studies of relatively low-barrier processes [27,28] relying on gas phase systems or long MD simulations, in this work, we propose an approach, suited to high-barrier reactive processes, that employs MLIPs trained with unbiased TPS data, to accurately predict both thermodynamic equilibrium constants and kinetic rates. In this method, AIMD calculations are only required to build a training set, all the rest being taken care of by the MLIP. Our method incorporates several previously mentioned enhanced sampling techniques, most notably metadynamics, TPS, and umbrella sampling. The workflow is summarized in Fig. 1. In this scheme, unlike previous works, our training method relies solely on unbiased trajectories starting from the top of the barrier, relaxing into the reactants and products basins. This means that all the information necessary to describe a reactive process is contained within the TPS simulations which is one of the key results of this study. This allows CV tuning without retraining the MLIPs. Furthermore, our MLIP training does not demand detailed prior knowledge of the reaction mechanism.

We demonstrate the effectiveness of our proposed approach by applying it to the extensively studied S_N2 substitution reaction, where a chlorine atom in the methyl-chlorine molecule is substituted by a chloride ion previously solvated [29–31]. The composition of the simulation box can be found in the Supplemental Material [32]. Comparing our MLIP-generated free energy profiles with *ab initio* calculations reveals excellent agreement. Furthermore, we employ the Bennett-Chandler formalism to compute exact kinetic rates, accounting for recrossing events not captured by transition state theory (TST).

Generation of the dataset and training the models. In order to run TPS shootings, a first transition trajectory is obtained using metadynamics. To measure the progress of the reaction, we use a path CV (indicated with s_2) defined only on two references (the reactants and the products) [33,34], employing as metric the square of the Euclidean distance between the coordination patterns of the reactive atoms of the current frame and the reference ones (see the Supplemental Material [32] for more information). This includes solvent effects, and has already been successfully used in many studies [7,35,36]. After obtaining an approximate free energy landscape, this variable is used to locate the barrier-top region in the “shooting from top scheme.” At convergence, the unbiased mechanism—possibly different from the first guess—is sampled. For this specific reaction, a simple CV is often used in the literature [13,29–31]: the difference between the two chlorine-carbon distances, indicated with $d_1 - d_2$. We will also consider it in this work to compare with previous studies.

Using TPS, 220 unbiased trajectories bridging reactants and products are generated. This gives us a variety of transition paths and TS that describe well the transition path ensemble. We used the 54 accepted trajectories as a training set. In Fig. 2 the TPS trajectories are projected on the two aforementioned CVs: $d_1 - d_2$ and s_2 .

These trajectories contain different unbiased reactive paths, which, as we will demonstrate, grasp the whole diversity of the atomic environment of the reactive atoms and the solvent during the reaction. This is the key to training a MLIP which relies on the representation of local atomic environments. Therefore, we used these TPS trajectories as training data along with the method we devised in a recent work [8]. To do so, we use the DEEPM smooth-edition package [37,38]

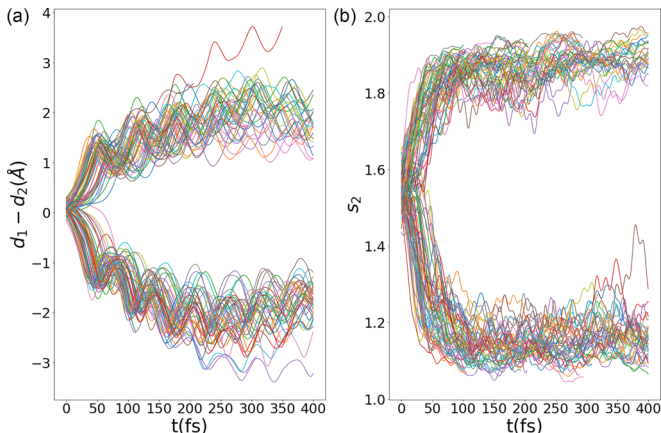


FIG. 2. TPS training trajectories projected on different CVs: (a) the difference between the two chlorine-carbon distances, $d_1 - d_2$, and (b) the path CV s_2 defined over the two reference states represented by reactants and products.

which is based on a Behler-Parrinello [17] structure. In these models, the total energy of the system is expressed as a sum of individual atomic contributions, each of these is computed using a separate neural network, with the condition that the neural networks associated to atoms of the same species have the same weights to ensure permutation invariance. The input of each neural network must respect the symmetries of the system, which is why descriptors are used. In this package, they are computed using an embedding neural network [37]. To deal with the heterogeneity of the system, that is intrinsic to reactions in solution, and to avoid water molecules to have an overwhelming weight in the training of the potential, we use a custom loss function to optimize the neural networks weights, which is defined by Eq. (1):

$$L(\mathbf{w}) = \frac{1}{|B|} \sum_{l \in B} \left[p_E |E_l - E_l^w|^2 + p_f \frac{1}{N_{\text{elem}}} \sum_{i=1}^N \frac{1}{n_i} |\mathbf{F}_{l,i} - \mathbf{F}_{l,i}^w|^2 \right], \quad (1)$$

where n_i is the number of atoms of the same element as atom i in the system, N_{elem} is the number of different elements in the system, E_l and $F_{l,i}$ denote the DFT energies and forces of the training set, while E_l^w and $F_{l,i}^w$ are the forces and energies computed by the MLIP, and B is the batch size (i.e., the number of trajectory frames). \mathbf{w} denotes the set of parameters of the neural networks. By weighting with n_i^{-1} the force-related terms, we ensure that each atomic species has the same weight in the training process.

Umbrella sampling simulations and validation of the model. As explained above, in order to obtain the full free energy profile along a RC, US simulations are performed. In this method, the space is divided into bins called windows, in which a quadratic potential is introduced to force the system to stay within the vicinity of the center of the window. Then, all the statistics from all the simulations are gathered to get the free energy profile using the weighted histogram analysis method (WHAM). In the rest of this work, we use 60 windows with a

spring constant defined by $k = k_B T / (\Delta s / 2.5)^2$, where Δs is the space between the center of two adjacent windows. All the molecular dynamics simulations were performed using code LAMMPS [39] patched with plumed 2.5 [40,41]. A timestep of 0.5 fs was used along with a Nosé-Hoover chain thermostat with a target temperature of 300 K. At the end of the process, the data points are carefully examined to avoid any hysteresis effect in the transition. All the free energy profiles are computed with the WHAM algorithm implemented in the Grossfield code [42]. In order to assess uncertainty in the FES estimation, the simulations are sliced in four, the two first are discarded as equilibration while the free energy is computed independently on the last two. The difference between these two profiles provides us the statistical uncertainty. The free energies were computed using 150 bins and a tolerance of 10^{-7} .

At first, we assess the quality of the training set by quantifying the ability of our MLIP to recover thermodynamics data. To do so, we perform US simulations on the $d_1 - d_2$ CV with different training sets. For each training set, we train a committee of four neural networks [43] that differ only on the random seeds that are employed for training. During a simulation, at time t , we use the following disagreement on the prediction of the forces as a metric for the accuracy of the prediction:

$$\sigma_{\text{max}}(t) = \max_{i \in [1, N_{\text{atoms}}]} \sqrt{\sum_{k=1}^{N_C} |\mathbf{F}_{i,t}^{(k)} - \overline{\mathbf{F}}_{i,t}|^2}, \quad (2)$$

where $N_C = 4$ is the size of the committee, $\mathbf{F}_{i,t}^{(k)}$ is the force predicted for atom i by committee member k , and $\overline{\mathbf{F}}_{i,t}$ is the average prediction of the committee. As explained in Ref. [8], σ_{max} is also used to perform a ‘‘mirror reflection’’ keeping the simulation within the region in which MLIP forces are reliably estimated. The results obtained with the different MLIPs are presented in Fig. 3. The free energy obtained with an insufficient number of training trajectories is quite far from the reference AIMD one, but, as the number of training TPS trajectories increases, the MLIP gives a better and better approximation of the reference free energy. In the end, we kept the MLIP with 60 training trajectories as it seemed convergence had been reached, in the sense that adding more configurations in the training set did not increase the accuracy of the predictions. In the following of this work, we use this MLIP, which satisfactorily reproduces the *ab initio* results for a significantly lesser computational cost. The difference between the barrier found with *ab initio* and MLIP calculation might be explained by the fact that more simulations were performed with the MLIP. This hypothesis is also supported by the free-energy difference between the reactants and the products: since the reaction is symmetric, it should be zero, while it is not in the AIMD case due to insufficient sampling.

Committer analysis. A crucial point in the atomistic study of chemical reactions and structural transformation is the analysis of transition pathways and TS. A rigorous method for identifying TS relies on committer analysis. This involves initiating a large number of unbiased trajectories from a presumed TS configuration with initial velocities randomly picked from the Maxwell-Boltzmann distribution. By doing

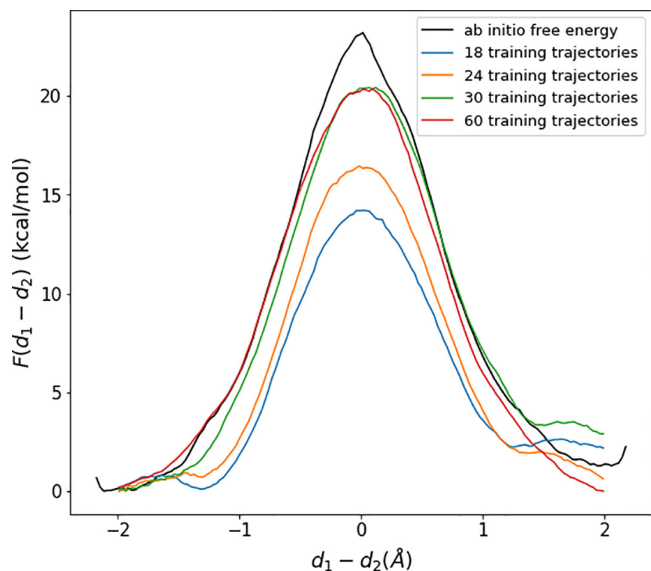


FIG. 3. Free energy along the $d_1 - d_2$ collective variable for a training set made of 18 (blue), 24 (orange), 30 (green), and 60 (red) training trajectories compared with the reference *ab initio* free energy (black).

so, the probability of transitioning from this configuration to the product state can be calculated by determining the ratio of trajectories reaching the products to the total number of trajectories. This computation yields the committor probability, denoted as q , and a TS is defined as a configuration with $q = 0.5$. However, in the majority of *ab initio* studies, the computational demands of such techniques are so substantial that the selection of candidate configurations is minimized, and frequently, the number of shooting trajectories is limited to around ten [7,44]. In contrast, using our MLIP, we initiated 500 trajectories from a total of 1196 configurations in the training set, each with random initial velocities. The resulting analysis is presented in Fig. 4, displaying the calculated q values along the $d_1 - d_2$ collective variable. This approach provides a clear understanding of the transition mechanism

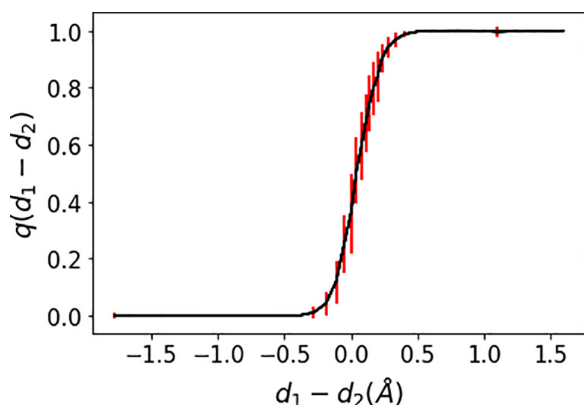


FIG. 4. Empirical committor function q as a function of $d_1 - d_2$ computed on configurations from the training set. Data points were put into bins, the error bars correspond to the standard deviation of the empirical committor within each bin.

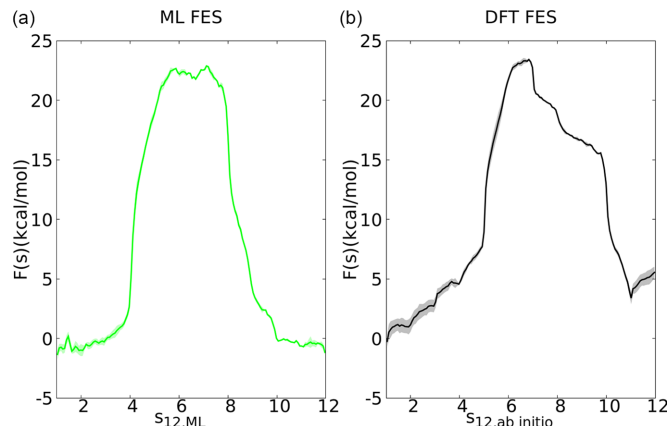


FIG. 5. (a) Free-energy landscape based on MLIP-US simulations along a path CV devised with MLIP-TPS reference frames ($s_{12,ML}$). (b) The corresponding landscape obtained using *ab initio* US along a path CV devised with *ab initio* TPS reference frames ($s_{12,ab initio}$).

along this collective variable and, as expected, we observe that the point where $q=0.5$ corresponds to $d_1 - d_2 = 0.0$.

Thanks to the unbiased nature of the training set, the MLIP can be used in combination with another CV without retraining. Moreover, it can also be used to perform additional TPS shootings. We thus expanded the *ab initio* dataset, and from these trajectories, frames were chosen according to the protocol defined in Ref. [13] to define a more detailed path CV [33], $s_{12,ML}$. We then performed new US simulation along this path CV.

The results, presented in Fig. 5, indicate that the MLIP-based free-energy profile along $s_{12,ML}$ compares well with the corresponding *ab initio* one, as well as with the one computed along the heuristic CV $d_1 - d_2$.

We have thus demonstrated that MLIP-driven free-energy profiles comparable to *ab initio* ones can be obtained for a significantly lesser computational cost: 60 MLIP-US simulations (20 ps per window) required 12 000 CPU.h on Intel Cascade Lake 6248 processors, while *ab initio* ones required 864 000 CPU.h. The most expensive part of the ML protocol (140 000 CPU.h) is the generation of the *ab initio* training set.

Computation of the rate constant. A major challenge in the study of chemical reactions is the calculation of realistic rate constants. Indeed, they are seldom computed in *ab initio* studies taking into account recrossing events, because of the formidable computational burden.

In principle, a well-known approach is the reactive-flux definition of the rate [9,45], employing unbiased trajectories started close to the barrier top, $q(0) = q^*$ (with q the chosen CV):

$$k^{RF}(t) = \frac{\langle \dot{q}(0) \delta(q(0) - q^*) h_B(q(t)) \rangle}{\langle h_A \rangle}, \quad (3)$$

where $\dot{q}(0)$ is the value of the CV derivative at the start of the simulation, q^* is the value of the CV at the TS, and $h_{B,A}$ are indicator function of reactants A and products B, respectively. This correlation function should reach a plateau for times larger than the typical molecular time scale. The rate can be evaluated by generating N trajectories starting close to the

TABLE I. Transmission coefficient κ obtained from *ab initio* TPS (500 shootings) or MLIP-based TPS (5475 shootings). As the reaction is symmetric, we took the average over forward/backward transitions, and the uncertainty was assessed as the deviation between the two directions.

	Machine learning	<i>Ab initio</i>
κ for $d_1 - d_2$	0.498 ± 0.009	0.54 ± 0.05
κ for $s_{12,ML}$	0.25 ± 0.02	0.25 ± 0.08

barrier top, knowing the free-energy profile $F(q)$:

$$k^{RF}(t) = \frac{\sum_{i=1}^N \dot{q}_i(0) h_B(q_i(t))}{N} \frac{e^{-\beta F(q^*)}}{\int_{\Omega_A} e^{-\beta F(q)} dq}, \quad (4)$$

where Ω_A is the reactants domain. The first term is extremely expensive to compute, as it typically needs 10^3 – 10^5 trajectories to reach statistical convergence (this is the main reason why less-accurate TST is often used instead). In the latter formula, the barrier term and the trajectory average term are both potential sources of error for the MLIP rate. Hence, to validate the calculation of kinetic rates using MLIPs, we will first compute the transmission coefficient κ , which also characterizes the deviation of the system from transition state theory

$$\kappa = \frac{k^{RF}}{k^{TST}} = \frac{\sum_{i=1}^N \dot{q}_i(0) h_B(q_i(t))}{\sum_{i=1}^N \theta(q - q^*) \dot{q}_i(0)}. \quad (5)$$

It is commonly considered that better reaction coordinates (i.e., close to the committor, ideal coordinate) have a relatively large κ , while poor CVs have a smaller κ [46]. To compute the rate constant, and the transmission coefficient, we performed 5475 MLIP-TPS shootings. The *ab initio* values are computed using 500 shootings. The values of κ are reported in Table I: MLIP and *ab initio* results are similar within error bars. This means that the kinetic information obtained with the MLIP is consistent with the *ab initio* behavior. Moreover, the values obtained here are close to the ones given in Ref. [31] of 0.39 ± 0.07 for $d_1 - d_2$, thus supporting the validity and strength of our method. The values of κ also allow us to compare the quality of the CV. Here, κ is almost twice as high for $d_1 - d_2$ than for $s_{12,ML}$ which means that $d_1 - d_2$ should be a better collective variable than the path CV. This is also the conclusion we reached in Ref. [13] by using a criterion based on the committor.

Using all the methods listed above, we report the most important, experimentally measurable quantities in Table II. The small difference (1–2 kcal/mol, i.e., 2–3 $k_B T$) between *ab initio* and MLIP barriers is enough to explain the discrepancy between the corresponding rate values (due to their exponential relation). The difference between the values reported in this work and the ones from other numerical

TABLE II. Relevant thermodynamic and kinetic quantities: the equilibrium constant K^{eq} , the barrier height ΔF^\ddagger , and the kinetic rate k . For the estimation of ΔF^\ddagger and k , the free energy profile was symmetrized, since reactants and products are the same species (giving a theoretical $K^{eq} = 1$).

	Machine learning	<i>Ab initio</i>
K^{eq} for $d_1 - d_2$	0.8 ± 0.6	0.06 ± 0.07
K^{eq} for s_{12}	0.7 ± 0.4	0.03 ± 0.04
ΔF^\ddagger for $d_1 - d_2$	20.0 ± 0.6 kcal/mol	22.5 ± 0.2 kcal/mol
ΔF^\ddagger for s_{12}	23.0 ± 0.4 kcal/mol	23.6 ± 0.7
κ for $d_1 - d_2$	$(6 \pm 2) \times 10^{-3} \text{ s}^{-1}$	$(3 \pm 4) \times 10^{-4} \text{ s}^{-1}$
κ for $s_{12,ML}$	$(1.0 \pm 0.7) \times 10^{-5} \text{ s}^{-1}$	$(3 \pm 2) \times 10^{-5} \text{ s}^{-1}$

studies [31] could probably be explained by the difference in electronic structure calculation methods, particularly the difference in the exchange-correlation functional used or the QM/MM method.

The reaction being symmetric, it is experimentally hard to characterize the activation barrier, it was, however, indirectly computed by interpolating the activation barrier of nonsymmetric reactions of the same type and the value commonly accepted is 26.5 kcal/mol [47,48]. The discrepancy observed between this work and the experimental value is likely to be due to DFT inaccuracy rather than a MLIP error, since it was also observed with DFT calculations. Overall, with the MLIP we performed two sets of US simulations and 5475 TPS shootings, for a total of 3.5 ns of simulations and a cost of 167 400 CPU.h (including the training set generation). If this study was performed fully *ab initio*, the total CPU time used would be 2 448 000 CPU.h.

Conclusion. In conclusion, this Letter demonstrates the remarkable capability of MLIPs, trained by using one batch of short, out-of-equilibrium, and computationally affordable trajectories, originating from the TS of rare events. Leveraging US and TPS simulations, we have proven that this MLIP is highly effective in computing experimentally relevant quantities, such as free energies and kinetic rates.

The breakthrough achieved in this study paves the way for the description of intricate and elusive phenomena, such as more complex chemical reactions in solutions, crystal nucleation, or structural phase transitions, with *ab initio* level accuracy, while significantly reducing computational costs, opening up new avenues for ML-based research in computational condensed matter and materials science.

Acknowledgments. This work was granted access to the HPC resources of IDRIS (Institut du Développement et des Ressources en Informatique Scientifique) under the allocations 2022-A0120901387 and 2023-A0140910387 attributed by GENCI (Grand Equipement National de Calcul Intensif). This work has been supported by the institute of computing and data sciences (ISCD) of Sorbonne University which funds L. Huet's thesis.

- [1] B. Cheng, S. Hamel, and M. Bethkenhagen, *Nat. Commun.* **14**, 1104 (2023).
 [2] A. Pérez-Villa, A. M. Saitta, T. Georgelin, J.-F. Lambert, F. Guyot, M.-C. Maurel, and F. Pietrucci, *J. Phys. Chem. Lett.* **9**, 4981 (2018).

- [3] F. Pietrucci, *Rev. Phys.* **2**, 32 (2017).
 [4] A. Laio and F. L. Gervasio, *Rep. Prog. Phys.* **71**, 126601 (2008).
 [5] G. M. Torrie and J. P. Valleau, *J. Comput. Phys.* **23**, 187 (1977).
 [6] A. Pérez-Villa, F. Pietrucci, and A. M. Saitta, *Phys. Life Rev.* **34-35**, 105 (2020).

- [7] T. Magrino, F. Pietrucci, and A. M. Saitta, *J. Phys. Chem. Lett.* **12**, 2630 (2021).
- [8] T. Devergne, T. Magrino, F. Pietrucci, and A. M. Saitta, *J. Chem. Theory Comput.* **18**, 5410 (2022).
- [9] D. Chandler, *J. Chem. Phys.* **68**, 2959 (1978).
- [10] P. G. Bolhuis, D. Chandler, C. Dellago, and P. L. Geissler, *Annu. Rev. Phys. Chem.* **53**, 291 (2002).
- [11] K. Palacio-Rodriguez and F. Pietrucci, *J. Chem. Theory Comput.* **18**, 4639 (2022).
- [12] H. Jung, R. Covino, A. Arjun, C. Leitold, C. Dellago, P. G. Bolhuis, and G. Hummer, *Nat. Comput. Sci.* **3**, 334 (2023).
- [13] T. Magrino, L. Huet, A. M. Saitta, and F. Pietrucci, *J. Phys. Chem. A* **126**, 8887 (2022).
- [14] B. Peters and B. L. Trout, *J. Chem. Phys.* **125**, 054108 (2006).
- [15] L. Mouaffac, K. Palacio-Rodriguez, and F. Pietrucci, *J. Chem. Theory Comput.* **19**, 5701 (2023).
- [16] H. Jung, K.-i. Okazaki, and G. Hummer, *J. Chem. Phys.* **147**, 152716 (2017).
- [17] J. Behler and M. Parrinello, *Phys. Rev. Lett.* **98**, 146401 (2007).
- [18] A. P. Bartók, M. C. Payne, R. Kondor, and G. Csányi, *Phys. Rev. Lett.* **104**, 136403 (2010).
- [19] A. P. Bartók, R. Kondor, and G. Csányi, *Phys. Rev. B* **87**, 184115 (2013).
- [20] A. Musaelian, S. Batzner, A. Johansson, L. Sun, C. J. Owen, M. Kornbluth, and B. Kozinsky, *Nat. Commun.* **14**, 579 (2023).
- [21] D. Lu, H. Wang, M. Chen, L. Lin, R. Car, W. E, W. Jia, and L. Zhang, *Comput. Phys. Commun.* **259**, 107624 (2021).
- [22] V. Kapil, C. Schran, A. Zen, J. Chen, C. J. Pickard, and A. Michaelides, *Nature (London)* **609**, 512 (2022).
- [23] Y. Zuo, C. Chen, X. Li, Z. Deng, Y. Chen, J. Behler, G. Csányi, A. V. Shapeev, A. P. Thompson, M. A. Wood, and S. P. Ong, *J. Phys. Chem. A* **124**, 731 (2020).
- [24] M. Yang, L. Bonati, D. Polino, and M. Parrinello, *Catal. Today* **387**, 143 (2022).
- [25] T. A. Young, T. Johnston-Wood, V. L. Deringer, and F. Duarte, *Chem. Sci.* **12**, 10944 (2021).
- [26] M. Bocus, R. Goeminne, A. Lataire, M. Cools-Ceuppens, T. Verstraelen, and V. Van Speybroeck, *Nat. Commun.* **14**, 1008 (2023).
- [27] M. Kulichenko, K. Barros, N. Lubbers, Y. W. Li, R. Messerly, S. Tretiak, J. S. Smith, and B. Nebgen, *Nat. Comput. Sci.* **3**, 230 (2023).
- [28] N. Gerrits, K. Shakouri, J. Behler, and G.-J. Kroes, *J. Phys. Chem. Lett.* **10**, 1763 (2019).
- [29] B. Ensing, E. J. Meijer, P. E. Blöchl, and E. J. Baerends, *J. Phys. Chem. A* **105**, 3300 (2001).
- [30] J. Chandrasekhar, S. F. Smith, and W. L. Jorgensen, *J. Am. Chem. Soc.* **106**, 3049 (1984).
- [31] C. Leitold, C. J. Mundy, M. D. Baer, G. K. Schenter, and B. Peters, *J. Chem. Phys.* **153**, 024103 (2020).
- [32] See Supplemental Material at <http://link.aps.org/supplemental/10.1103/PhysRevE.110.L033301>, which includes additional information.
- [33] D. Branduardi, F. L. Gervasio, and M. Parrinello, *J. Chem. Phys.* **126**, 054103 (2007).
- [34] F. Pietrucci and A. M. Saitta, *Proc. Natl. Acad. Sci. USA* **112**, 15030 (2015).
- [35] A. France-Lanord, F. Pietrucci, A. M. Saitta, J.-M. Tarascon, A. Grimaud, and M. Salanne, *PRX Energy* **1**, 013005 (2022).
- [36] G. Cassone, F. Saija, J. Sponer, J. E. Sponer, A. Jiménez-Escobar, A. Ciaravella, and C. Cecchi-Pestellini, *Mon. Notices Royal Astron. Soc.* **504**, 1565 (2021).
- [37] L. Zhang, J. Han, H. Wang, W. Saidi, R. Car, and W. E, End-to-end Symmetry Preserving Inter-Atomic Potential Energy Model for Finite and Extended Systems, *Advances in Neural Information Processing Systems* (2018), https://papers.nips.cc/paper_files/paper/2018/hash/e2ad76f2326fbc6b56a45a56c59fafdb-Abstract.html.
- [38] H. Wang, L. Zhang, J. Han, and W. E, *Comput. Phys. Commun.* **228**, 178 (2018).
- [39] S. Plimpton, *J. Comput. Phys.* **117**, 1 (1995).
- [40] M. Bonomi, G. Bussi, C. Camilloni, G. A. Tribello, P. Banáš, A. Barducci, M. Bernetti, P. G. Bolhuis, S. Bottaro, D. Branduardi, R. Capelli, P. Carloni, M. Ceriotti, A. Cesari, H. Chen, W. Chen, F. Colizzi, S. De, M. De La Pierre, D. Donadio *et al.*, *Nat. Methods* **16**, 670 (2019).
- [41] G. A. Tribello, M. Bonomi, D. Branduardi, C. Camilloni, and G. Bussi, *Comput. Phys. Commun.* **185**, 604 (2014).
- [42] A. Grossfield, WHAM: the weighted histogram analysis method version 2.0.10.2, http://membrane.urmc.rochester.edu/?page_id=126 (2022).
- [43] C. Schran, K. Brezina, and O. Marsalek, *J. Chem. Phys.* **153**, 104105 (2020).
- [44] F. Carrascoza, P. Lukasiak, W. Nowak and J. Blazewicz, *Astrophys. J.* **956**, 140 (2023).
- [45] S. Jungblut and C. Dellago, *Eur. Phys. J. E* **39**, 77 (2016).
- [46] R. G. Mullen, J.-E. Shea, and B. Peters, *J. Chem. Theory Comput.* **10**, 659 (2014).
- [47] W. J. Albery and M. M. Kreevoy, *Adv. Phys. Org. Chem.* **16**, 87 (1978).
- [48] S. Elliott and F. S. Rowland, *J. Atmos. Chem.* **20**, 229 (1995).